

Orbital rotational motion and turbulence below laboratory wind water waves

Jacques Magnaudet and Laurent Thais

Institut de Mécanique des Fluides de Toulouse, Unité de Recherche Associée au CNRS, Toulouse, France

Abstract. New experimental results describing the structure of both orbital and turbulent motions below laboratory wind water waves are presented. The data obtained by means of a submersible laser probe are processed through the triple decomposition method developed by the authors. This method allows one to distinguish three contributions in the fluctuating motion, namely the potential and rotational parts of the orbital motion, as well as the turbulent fluctuation. The results show that the orbital rotational motion has spectral properties very similar to those of its potential counterpart and represents a contribution of significant magnitude. The behavior of all three components of the turbulent motion is discussed. Their near-surface level is comparable with that found near a wall, but their vertical decay is quite different. The dissipation rate estimate confirms that under present conditions the turbulence is essentially unaffected by the orbital motion. In contrast, a study of the cross correlations between orbital rotational and potential motions shows that the rotational contribution plays a key role in energy transfers between the wave motion and the mean shear flow. Finally, the origin of the orbital rotational motion is addressed. Several theoretical mechanisms capable of contributing to the generation of a wave-related component of the vorticity are examined. Comparison between theory and experiments supports the idea that in laboratory experiments an important part of the orbital rotational motion results from wave-current interactions linked to the vertical variations of the mean shear.

1. Introduction

Interactions between wind-generated waves, wind-induced mean current, and turbulence affect significantly the dynamics of the surface layer of the ocean and are thus of particular importance for predicting transfers through the top meters of water. These interactions are extraordinarily complex since they involve many different processes like turbulence production by breaking, propagation of the wave field on a nonuniform shear, forcing of the turbulent motion by the orbital motion, etc. Even though the importance of several of these mechanisms has been earlier recognized, present knowledge is quite unsatisfactory because precise and complete experimental data are, as yet, rather rare while available theoretical studies only concern some aspects of the problem. Nevertheless, among many experimental studies carried out in the field or in laboratory tanks (see *Cheung and Street* [1988] for a review), several characteristics of the water motion have emerged.

Kitaigorodskii et al. [1983] performed field measurements on Lake Ontario and found that the level of both the turbulent kinetic energy and its dissipation rate were dramatically increased with respect to usual shear flows. This finding means that turbulence below wind waves does not originate entirely in shear production but that other mechanisms usually termed as "wave-turbulence interactions" also act. The same authors also found that turbulent spectra exhibited a bump near the dominant wave frequency. *Lumley and Terray* [1983] analyzed these spectra and explained their form by a kinematic model in

which turbulent fluctuations are transported bodily by the mean current and the orbital motion. A similar form of the spectra was also observed in laboratory experiments [*Terray and Bliven*, 1985], and the authors found a good agreement with the model of *Lumley and Terray* [1983].

The phase relation between the surface displacement and the orbital motion was also investigated. *Cavaleri and Zecchetto* [1987] established in sea measurements that under swell conditions, orbital velocities obey the standard theory, while a downward momentum flux exists under active wind conditions. This momentum flux is a clear indication of the existence of a rotational component in the orbital motion. Most of the foregoing features were also observed in laboratory experiments by *Cheung and Street* [1988]. These authors studied both wind-generated waves and mechanical waves sheared by a wind. They established the existence of a positive cross correlation between the horizontal and the vertical orbital velocities, indicating an energy transfer from the waves to the mean current. Furthermore, they found a strong increase of the turbulent kinetic energy level in presence of mechanically generated waves, suggesting that significant wave-turbulence interactions can be observed under certain conditions in laboratory experiments and that some aspects of these interactions are certainly related to the cross correlation of the orbital velocities.

In every experimental study dealing with turbulence below water waves, the question of separating the total velocity fluctuation into orbital and turbulent contributions is crucial; no analysis of the interactions between both contributions is possible before a decomposition process has been defined. Most of the studies previously mentioned made use of the well-known linear filtration technique (hereinafter referred to as LFT) of *Benilov and Filyushkin* [1970]. This method enables one to obtain very interesting information about the main

Copyright 1995 by the American Geophysical Union.

Paper number 94JC02715.
0148-0227/95/94JC-02715\$05.00

spectral features of orbital and turbulent motions. However, a major limitation of this technique lies in the linear relation assumed to exist between the surface displacement and the orbital motion. As a consequence, all nonlinearities of the orbital motion are rejected into the turbulent contribution. To overcome this shortcoming, *Jiang et al.* [1990] developed another technique based on a generalization of the Dean method [Dean, 1965] to random waves. They used this technique to reanalyze the wind wave data of *Cheung and Street* [1988]. Coherence spectra showed strong correlations between orbital and turbulent motions, leading the authors to the conclusion that marked wave-turbulence interactions exist below laboratory wind water waves. However, the separation criterion used by *Jiang et al.* [1990] is based on the severe assumption that the orbital motion is completely irrotational. Several experimental results including those of *Cavaleri and Zecchetto* [1987], as well as those obtained with mechanical waves by *Cheung and Street* [1988], do not support this assumption. This hypothesis is removed in the separation method thoroughly described in a companion paper by *Thais and Magnaudet* [this issue] (hereinafter referred to as TM). This method, called triple decomposition method (hereinafter referred to as TDM), is based on a decomposition of the fluctuating motion in which the determination of the potential orbital motion is achieved by means of an extension of the *Dean* [1965] method, while the rotational orbital motion and the turbulent fluctuation are computed by means of the LFT.

The main objective of this paper is to present new laboratory data analyzed with the aid of the TDM and to use the results to examine some aspects of wave-current and wave-turbulence interactions. Consequently, the remainder of the paper is organized as follows. In section 2 we present the characteristics of our facility and the experimental arrangement used to perform the experiments. Section 3 is devoted to the presentation of the results concerning the three contributions of the fluctuating motion. Section 4 discusses some consequences of the existence of an orbital rotational contribution and more generally of the orbital motion on the energetic balance of mean, orbital, and turbulent motions, while section 5 tries to distinguish the origin of the orbital rotational motion. The major conclusions are finally drawn in section 6.

2. Experiments

Experimental data were obtained in our laboratory wind-water tunnel facility. Dimensions of the channel are 22 m long, 1.2 m wide, and 2 m high. For all series of experiments the water depth was fixed to 1 m. Our facility offers the possibility to impose a mean water current ranging from 2 to 5 cm/s. During the experiments the air free-stream velocities ranged from 4.5 m/s to 13.5 m/s and the water current was set to 2 cm/s. All measurements were performed on the centerline of the channel at a fetch nearly equal to 13 m sufficiently far away from the dissipation beach.

Free-surface displacement with respect to the still water level was measured using a 300- μ m diameter, copper teflon capacitance gauge, while all three components of the instantaneous water velocity were successively measured by mean of a submersible one-component laser optical fiber system operating in backward scatter mode (in the remainder of the paper any fluctuating velocity component v_i will be denoted u , v , or w along the streamwise x , spanwise y , and vertical z direction,

respectively, the vertical axis being directed upward). The laser probe used was a 60X14 Dantec transducer whose complete technical specifications can be found in the Dantec 60X Fiber Flow Series Instruction Manual. The probe is a 14-mm diameter stainless steel head with 8 mm beam spacing and 66.7 mm focal length in water. The probe volume whose dimensions in water are 2.02 mm x 162 μ m with a green Ar-ion laser contains 37 fringes. The Doppler signal was processed with a 55N20 frequency tracker. Particular attention was paid to flow seeding in order to get a continuous signal output during the whole record. The capacitance gauge recording wave elevation was mounted at the same fetch as the LDV measuring volume but 2 mm away from it in the spanwise direction in order to avoid lighting of the wire or wake perturbations (Figure 1). Rotating the laser probe around the gauge axis, all three components of the water velocity were successively measured simultaneously with the wave elevation.

To ensure that laser head intrusion did not modify the behavior of the flow field, a systematic comparison of the results obtained either by the submersible fiber probe or by the outer classical optics proceeding in forward scatter mode was carried out. As an example, Figure 2 presents for a typical run the profiles of the vertical rms velocity obtained using both methods. The total fluctuation, as well as the orbital and turbulent contributions separated using the LFT, are shown in this figure. The collapse between both curves obtained for each contribution clearly proves that both intrusion of the probe and use of the backward scatter mode have no significant effect and that the present technique can be used with confidence.

At each wind regime a separate set of experiments was conducted to determine the phase speed of the dominant frequency of the wave field. For this purpose, the cross-spectra technique based on simultaneous measurement of wave heights from two capacitance gauges aligned with the wind direction was used.

Four wind regimes were studied using the arrangement previously described. The corresponding air free-stream velocities determined by use of a Pitot tube were 4.5 m/s, 6.8 m/s, 9.0 m/s, and 13.5 m/s. Table 1 summarizes the wave characteristics determined at each wind velocity and the corresponding values of normalizing parameters u_* (water friction velocity), \bar{u}_{ps} (rms orbital surface velocity) and z_η (wave depth) which are used in the presentation of the results. Wave-related parameters \bar{u}_{ps} and z_η are defined in section 3. Friction velo-

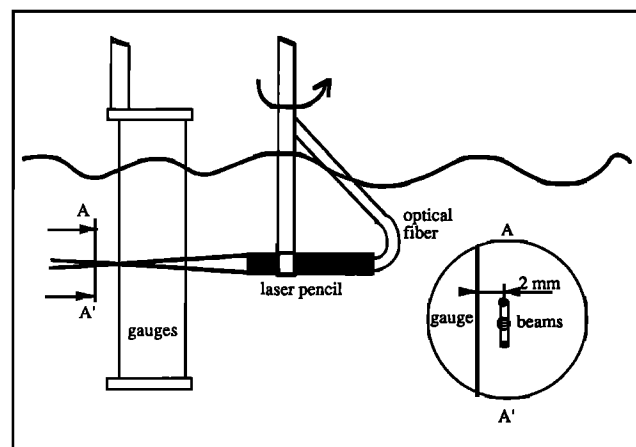


Figure 1. Detail of the experimental arrangement.

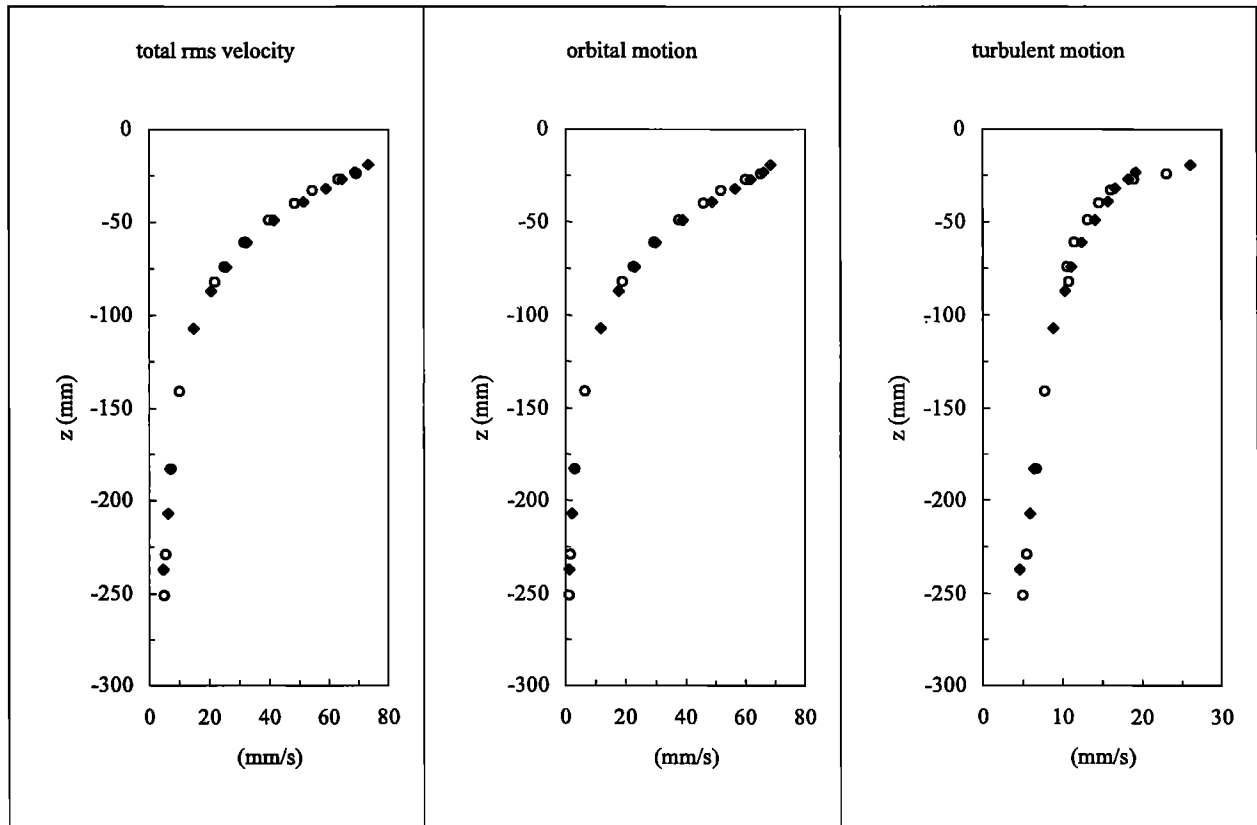


Figure 2. Comparison of vertical profiles of total, orbital, and turbulent rms velocities measured by means of external optics / forward scatter mode (open circles) and submersible probe / backward scatter mode (solid diamonds). (Wind speed $U_\infty=6.8$ m/s).

cities were taken from the experiments carried out by *Prodhomme* [1988] in the same facility. In these experiments, air friction velocities were first determined through a logarithmic fit of streamwise velocity profiles obtained from hot-wire measurements. Then, water friction velocities were obtained assuming continuity of shear stresses at the mean water level.

A Leuwen Measurements and Systems data acquisition system driven by an HP 1000-A700 real time computer was used to store the velocity and wave height signals. The sampling rate was 100 Hz and the sampling time 512 s for the analog to digital conversion.

3. The Three Contributions to the Fluctuating Motion

3.1. Separation Procedure

After the mean velocity \bar{V} is removed from velocity records by time averaging the fluctuating velocity data are processed using the triple decomposition method (TDM) described in TM. The reader is referred to TM for all points concerning the theoretical foundations of the method and the discussion of the physical assumptions on which it is based, as well as the validation tests. We just recall here the main ideas of the TDM. From any simultaneous measurement of the wave elevation η and the instantaneous velocity V at the same fetch the TDM first computes in a nonlinear way the velocity fluctuation \tilde{v}_p corresponding to the potential part of the orbital motion. To achieve this goal, the TDM assumes that the orbital motion is

two-dimensional and nondispersive and takes into account the effect of the streamwise mean drift $\bar{U}(z)$. Then, applying the LFT to $V - \bar{V} - \tilde{v}_p$, the spectral characteristics of both the rotational part of the orbital motion \tilde{v}_R and the turbulent fluctuation v' are simultaneously determined. It is crucial to notice that in this approach all the motions having a phase correlation with η lie into \tilde{v}_p or \tilde{v}_R , meaning that no phase correlation exists between η and v' . A consequence of this property is that no correlation can exist between v' and a contribution linearly related to the wave motion like \tilde{v}_R . Since nonlinear contributions in \tilde{v}_p are small (they were shown to be clearly smaller than \tilde{v}_R in TM) correlations like $\overline{\tilde{u}_{pi}v'_j}$ between the i th component of \tilde{v}_p and the j th component of v' are also almost zero.

Table 1. Physical Parameters of the Experiments

U_∞ m/s	u_* mm/s	f_0 Hz	c m/s	$(\overline{\eta^2})^{1/2}$ mm	\tilde{u}_{Pz} mm/s	z_η mm	R
4.5	7.6	3.6	0.61	3.4	67.1	18.5	8.8
6.8	11.7	2.8	0.73	5.8	92.7	30.0	7.9
9.0	17.3	2.4	0.85	7.8	98.3	38.6	5.7
13.5	27.6	2.0	1.06	14.0	144.2	61.6	5.2

Variables are defined as follows: U_∞ , wind speed; u_* water friction velocity; f_0 dominant wave frequency; c absolute phase velocity of the dominant wave; $(\overline{\eta^2})^{1/2}$ rms wave height; \tilde{u}_{Pz} rms orbital surface velocity; z_η wave decay depth; and $R = \tilde{u}_{Pz} / u_*$.

3.2. Linear and Nonlinear Orbital Potential Motions

The quantity first extracted from velocity measurements is the potential part of the orbital motion. To emphasize nonlinear effects, it is useful to consider separately the linear part \tilde{v}_{P1} of \tilde{v}_P and its nonlinear counterpart \tilde{v}_{P2} , the denominations linear and nonlinear referring to the kinematic and dynamic equations satisfied on the free surface by \tilde{v}_{P1} and $\tilde{v}_{P1} + \tilde{v}_{P2}$ respectively (see equations B2 and B3 of TM). Figure 3 shows for all experimental conditions the excellent data collapse of the linear streamwise orbital potential velocity arising from the TDM (the vertical component not shown here behaves similarly). The normalizing parameters are the rms surface orbital velocity \tilde{u}_{Ps} and the wave decay depth z_η , both deduced from linear wave theory. These parameters are defined the following way: generalizing the linear potential solution (see equation (A4b) of TM) to random waves by means of the wave energy spectrum $S_{\eta\eta}(f)$ and taking into account the assumption of a constant phase velocity used in the TDM, the characteristic rms value of the wave-induced potential motion at depth z is obtained as

$$\tilde{u}_{Pz} = 2\pi \frac{c_0}{c} \left[\int f^2 S_{\eta\eta}(f) \exp(4\pi f z / c) df \right]^{1/2} \quad (1)$$

where c and c_0 denote the absolute and relative phase velocities of the dominant wave, respectively. The surface orbital velocity \tilde{u}_{Ps} is the value given by (1) at $z=0$, whereas the decay depth z_η is the value of z at which $\tilde{u}_{Pz} / \tilde{u}_{Ps} = \exp(-1)$ (z_η is the inverse of the wave number for a sine wave). With this choice of normalizing parameters the single exponential decay found in Figure 3 results simply from the fact that most of the wave energy is located in a very narrow band of wavenumbers centered around the dominant wave.

The nonlinear part $(\tilde{u}_{P2}^2)^{1/2}$ and $(\tilde{w}_{P2}^2)^{1/2}$ of the potential wave-induced velocities (not shown here) decays with depth as $\exp(2z/z_\eta)$, meaning that it is principally due to the second harmonic of the dominant wave. The velocity \tilde{v}_{P2} is smaller than \tilde{v}_{P1} by more than 1 order of magnitude. Thus as discussed in subsection 3.5 of TM, the effects of both orbital rotational motion and turbulence must a priori be taken into account to evaluate \tilde{v}_{P2} . This is not the case in the TDM because the orbital potential motion has to be determined without knowing explicitly the other contributions. As a consequence, the characteristics of \tilde{v}_{P2} are probably only roughly resolved by the method.

3.3. Orbital Rotational Motion

Once \tilde{u}_P and \tilde{w}_P are extracted from the measured velocity component, the spectra of \tilde{u}_R and \tilde{w}_R are obtained in the second step of the TDM (equation (27) of TM). As shown in Figure 4 the shape of these spectra is very similar to that of the \tilde{v}_P spectra (see Figure 8 of TM for another example). The power spectra $S_{\tilde{v}_{Ri}\tilde{v}_{Ri}}$ present a sharp peak centered on the dominant wave frequency $f=f_0$ and follows essentially the same slope as $S_{\tilde{v}_{P1}\tilde{v}_{P1}}$ on both sides of f_0 . This means that the ratio of the spectral densities of \tilde{v}_R and \tilde{v}_P is nearly constant over the whole peak of the spectra. Vertical profiles of the rms of \tilde{u}_R and \tilde{w}_R are plotted on Figures 5a and 5b using the same normalizing parameters as in Figure 3. These figures suggest two essential comments. First of all, it appears that at a given wind speed the slopes of the \tilde{u}_R and \tilde{w}_R rms profiles are quite different. This is an important indication that \tilde{v}_R carries vorticity (see equation (34) of TM). Furthermore, it appears that \tilde{u}_R and \tilde{w}_R rms profiles do not collapse on a single curve. This could signify that the normalizing parameters used are not relevant. However, the theoretical analysis developed in section 5 provides another reason; it suggests that \tilde{v}_R is

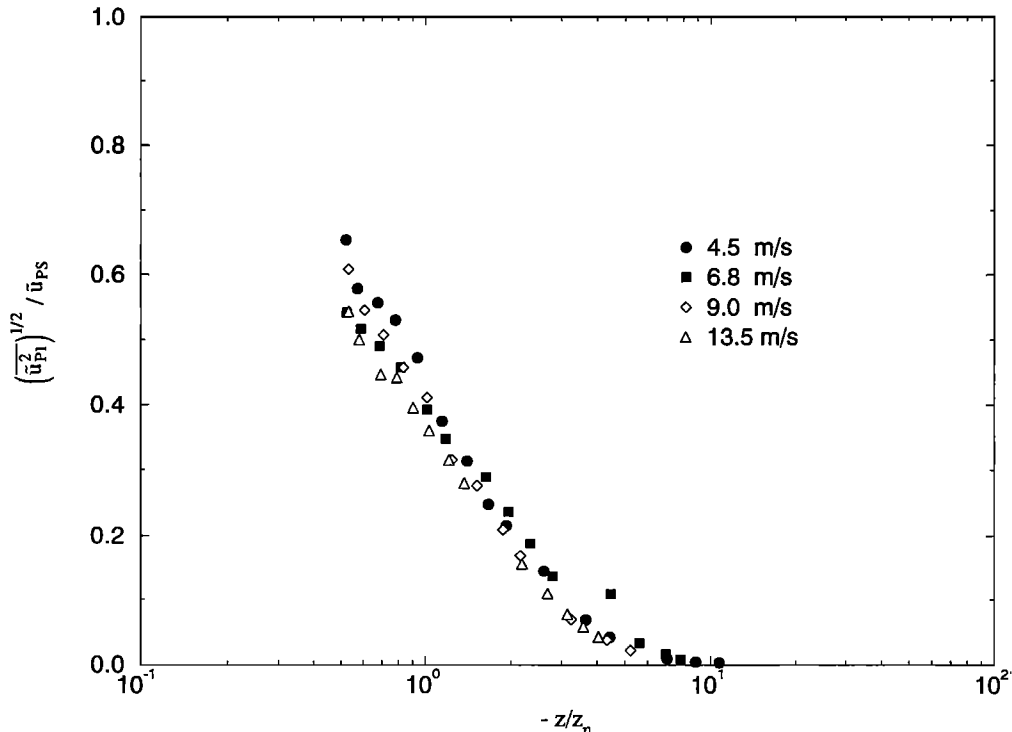


Figure 3. Linear part of the streamwise potential orbital velocity. Wind speed U_∞ is 4.5 m/s (solid circles); 6.8 m/s (solid squares); 9.0 m/s (open diamonds); 13.5 m/s (open triangles).

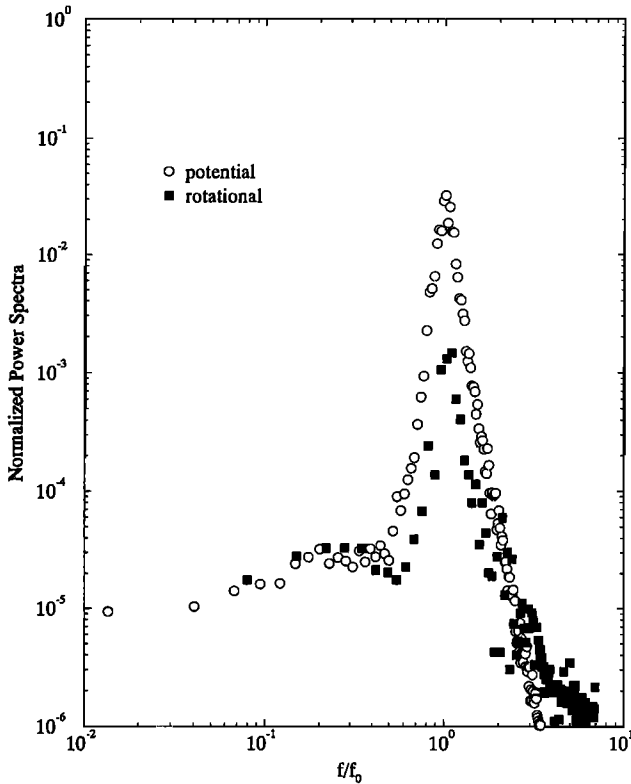


Figure 4. Typical spectra of the vertical wave-induced potential and rotational motions. (All velocity spectra are normalized by energy of the total fluctuation and integration time). Potential contribution is denoted by circles, rotational contribution by squares.

generated through different processes and that these processes involve several different scales, so that no universal normalizing parameter can be found. This lack of universality with respect to scales relevant for \tilde{v}_P is also an indication that \tilde{v}_R is not an artifact of the TDM like an orbital potential contribution forgotten in the first step of the method. Figures 5a and 5b also show that the order of magnitude of \tilde{v}_R is highly significant. Since the ratio $(\tilde{v}_{Ri}^2 / \tilde{u}_{Pz}^2)^{1/2}$ reaches values between 12 and 20% near the surface (depending on the component \tilde{u}_R or \tilde{w}_R under consideration), $(\tilde{v}_{Ri}^2 / \tilde{v}_{Pz}^2)^{1/2}$ lies between 20 and 30%, a level which is far beyond the limit of accuracy of the separation method. It is worth noting in particular that the kinetic energy associated with \tilde{v}_R is larger by roughly 1 order of magnitude than that associated with the nonlinear potential contribution \tilde{v}_{P2} . In other terms, the motion induced by laboratory wind waves seems to be "more" rotational than nonlinear.

3.4. Turbulent Motion

Figure 6 shows the typical behavior of the spectra of the turbulent contribution v' obtained in the second step of the TDM. They exhibit two prominent features. First of all, although all the orbital contributions have been removed by the successive extractions of \tilde{v}_P and \tilde{v}_R , a bump around the dominant wave frequency f_0 subsists on the u' spectra. Its magnitude decreases with the distance to the surface, as can be seen by comparing both spectra in Figure 6. This bump is also found on the w' spectra, but its magnitude is consistently much

smaller (see Figure 8 in TM). The second characteristic feature displayed by these spectra is related to the inertial zone; this zone with a slope nearly equal to $-5/3$ is found on both sides of the bump, but there is a systematic shift toward larger values of the spectral density for frequencies lying above the bump. Several of these trends have been observed by previous investigators, even if they obtained the turbulent contribution by different methods. *Donelan* [1978] obtained turbulent spectra by subtracting from the total fluctuation the wave-induced velocity deduced from linear wave theory. He suggested that the shift of spectral densities for $f > f_0$ was due to the existence of a source of turbulent energy near the wave peak. Moreover, he found that for $f > f_0$ the slope of the spectra approached $-5/2$, which could suggest a trend toward two-dimensionality of wave-induced turbulence. *Kitaigorodskii et al.* [1983] and *Terray and Bliven* [1985] treated their data by applying directly the LFT to the whole velocity fluctuation. They interpreted the very specific shape of the turbulent spectra in the framework of the kinematic model proposed by *Lumley and Terray* [1983]; these authors showed that if turbulence can be considered frozen with respect to the wave motion then the turbulent wave number spectrum can be inferred from the frequency spectrum via a generalized Taylor hypothesis involving both mean drift and wave-induced potential motion. This purely kinematic model leads to the occurrence of a bump in the frequency spectrum around f_0 and shows that in the inertial range the ratio of spectral densities above and below f_0 is a function of $(\tilde{u}_{Pz}^2)^{1/2} / \bar{U}(z)$. *Terray and Bliven* [1985] applied this model to their data and found a satisfactory agreement with their spectra. The same procedure applied to present data also shows a fairly good agreement concerning the spectral density shift between high and low frequencies. Thus it appears that the form of the turbulent frequency spectra cannot be seen as a proof of the existence of dynamic wave-turbulence interactions. Unfortunately, the question of the origin of the bump cannot be more deeply clarified here since this would require a direct determination of the turbulent wave number spectra which has not been achieved up to now.

Vertical profiles of $(\bar{u}'^2)^{1/2}$ and $(\bar{w}'^2)^{1/2}$ normalized by water friction velocity u_* and total water depth H are plotted on Figures 7a and 7b. Water depth H is used because no characteristic vertical length scale appears; neither z_η nor the viscous scale ν/u_* is relevant for turbulent quantities near a rough interface, and the boundary layer thickness cannot be defined properly for a reason explained below. Owing to this lack of suitable universal scale, profiles of each component do not exactly collapse on a single curve. As commonly found in boundary layers, the streamwise fluctuation is larger than the vertical one near the surface. Both fluctuations reach maximum values of about 2.5 and 2.0, respectively, in fairly good agreement with those reported by *Cheung and Street* [1988] and with the usual results found in turbulent boundary layers [*Klebanoff*, 1955]. On the basis of the assumption of a two-dimensional orbital motion, as justified in TM, the total fluctuation measured along the spanwise axis is supposed to belong to the turbulent motion. The spanwise component $(\bar{v}'^2)^{1/2}$ is shown in Figure 7c. Maximum values of $(\bar{v}'^2)^{1/2}$ are close to those found for $(\bar{u}'^2)^{1/2}$. It is clear that even small, the three-dimensionality of the wave field contributes to v' especially at the highest wind speed for which an increase of the v' level and a change in the form of the decay can be observed. In usual boundary layers the magnitude of the

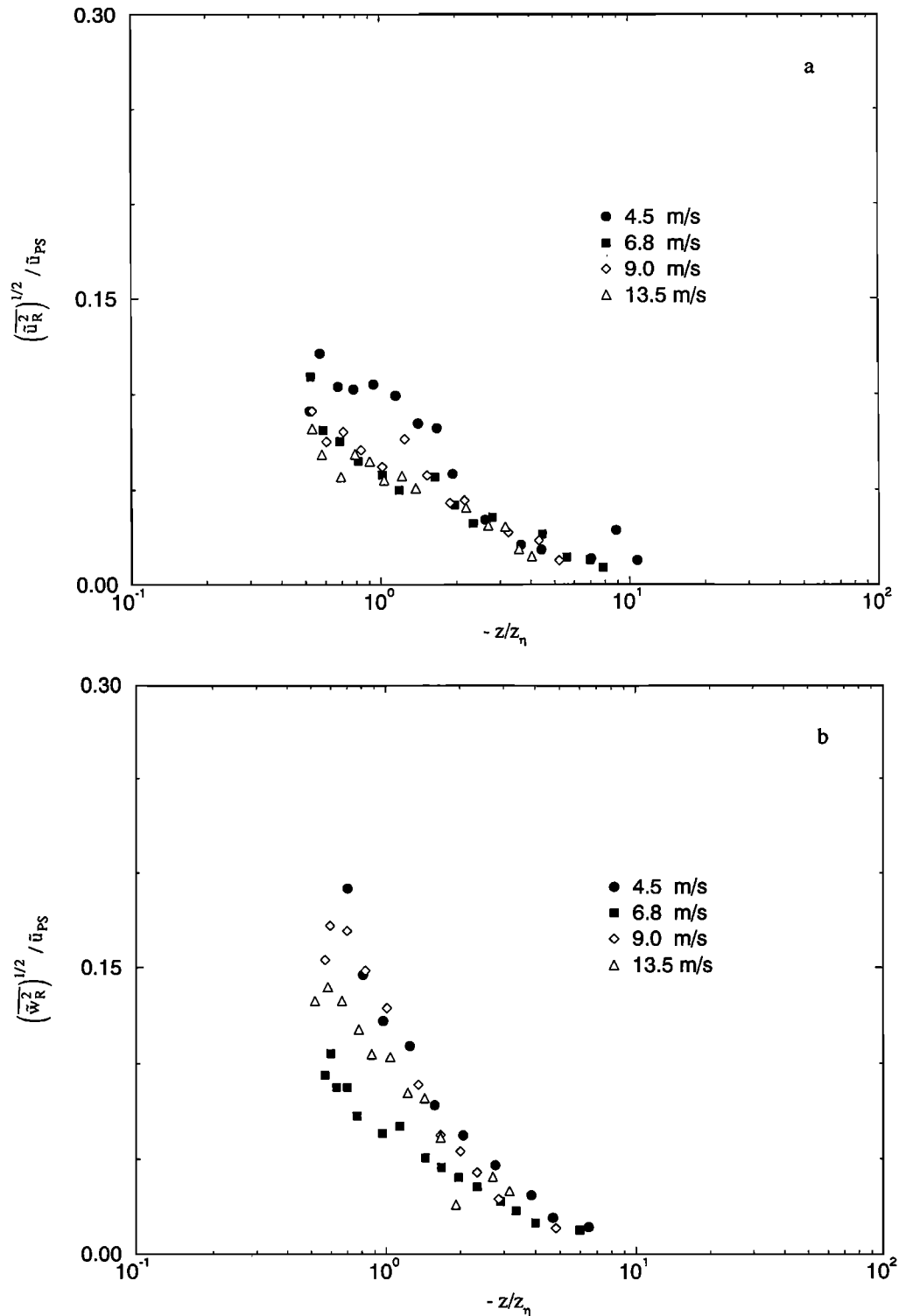


Figure 5. Vertical profiles of (a) \bar{u}_R and (b) \bar{w}_R .

spanwise fluctuation lies between the magnitude of the two other components. This suggests a way to estimate the magnitude of the spanwise component of the orbital motion. For example, at $U_w=13.5$ m/s the maximum excess of \bar{v}^2/u^2 with respect to the foregoing criterion is roughly $\Delta(\bar{v}^2/u^2) \approx 2.8$. Then, considering this excess as the orbital contribution, we get $\bar{v}^2/(\bar{u}^2 + \bar{v}^2 + \bar{w}^2) \approx 0.14$. Thus in the worst case only 14% of the wave kinetic energy lies in the

spanwise component. This percentage decays rapidly with U_w and can be considered as a confirmation of the weakness of three-dimensional effects in the wave field, a basic assumption for the validation of the TDM.

The various profiles of each component exhibit a rapid decay with depth following a law about $z^{-0.6}$. This behavior is quite similar to that reported by *Terray and Bliven* [1985], who found a z^{-1} decay of turbulent kinetic energy. In contrast, the

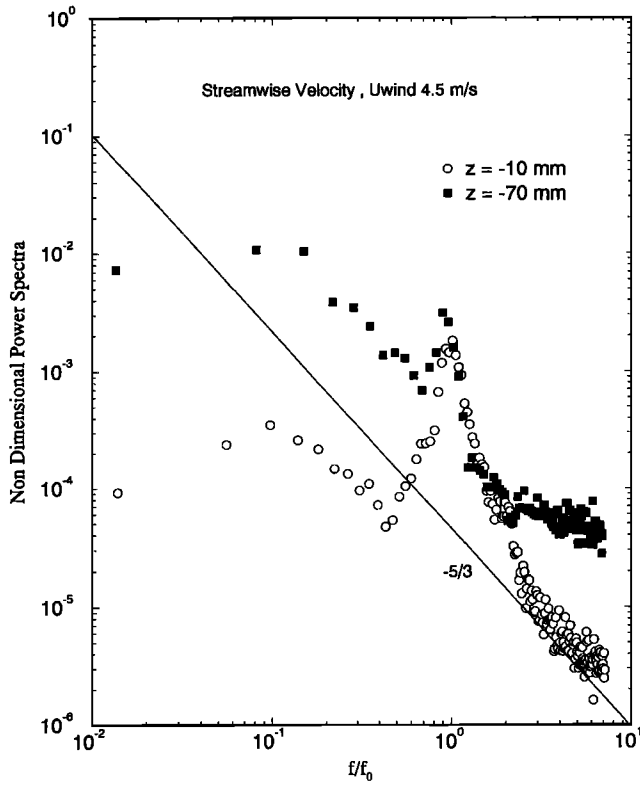


Figure 6. Typical spectra of the streamwise turbulent motion at two different depths. $z = -10$ mm (circles) and $z = -70$ mm (squares).

measurements of *Cheung and Street* [1988] exhibited a much slower decay. This difference is probably due to the existence of a pair of contrarotating cells in our wind-water facility as described by *Prodhomme* [1988]; these cells produce a small

but significant upwelling on the centerline of the channel (the order of magnitude of \bar{W} being typically 0.5 to 1 cm/s) and prevent diffusion of turbulence into the core of the flow. They also induce a strong nonlinearity of the shear stress $-\overline{u'w'}$ [*Prodhomme*, 1988]. That is the reason why it is hardly possible to define properly any length scale like the boundary layer thickness. These features illustrate the sensitivity of this kind of flow to the complex structure of the mean current.

4. Energy Transfers Between Mean, Orbital and Turbulent Motions

4.1. Balance Equations

Since the phase-averaging procedure defined by *Reynolds and Hussain* [1972] holds for a flow consisting of a periodic wave train superimposed on a turbulent motion, kinetic energy balances associated to the mean, orbital, and turbulent motions can be easily derived in such a case. The derivation is more complex for random waves since it depends on the definition of the orbital motion. One of the main advantages of the separation carried out by the TDM is to give balance equations of the mean, orbital, and turbulent contributions essentially identical to those obtained for periodic waves by the phase-averaging procedure [*Magnaudet*, 1989]. This results from the key point that the motion $\tilde{v}_p + \tilde{v}_R$ determined by the TDM contains almost all the characteristics of the orbital motion and especially the leading contribution to its vorticity as well as its main nonlinearity. For example, \tilde{v}_p satisfies a nonlinear Bernoulli equation (equation (16) of TM), so that terms like $1/2 \partial(\tilde{v}_{pi}\tilde{v}_{pi})/\partial x_j$ do not appear in the balance equation of v' , in contrast to the results of linear approaches like that of *Kitaigorodskii and Lumley* [1983]. Thus the only new terms that arise in the exact \bar{V} and v' balances (with respect to the equations obtained by phase-averaging) are only

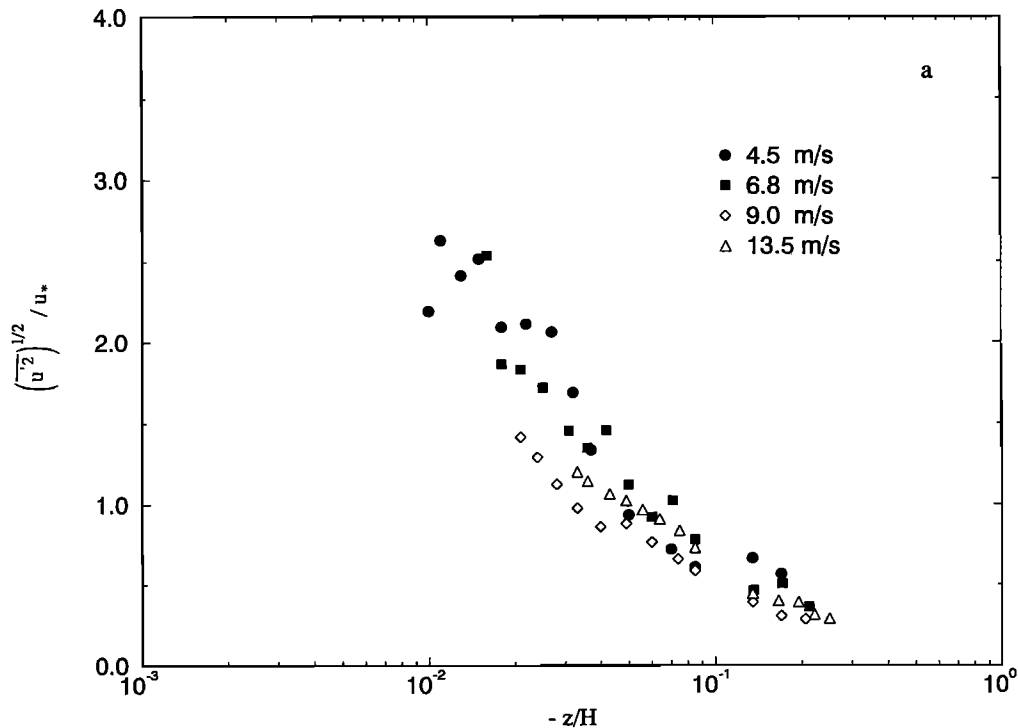


Figure 7. Vertical profiles of (a) u' , (b) w' , and (c) v' .

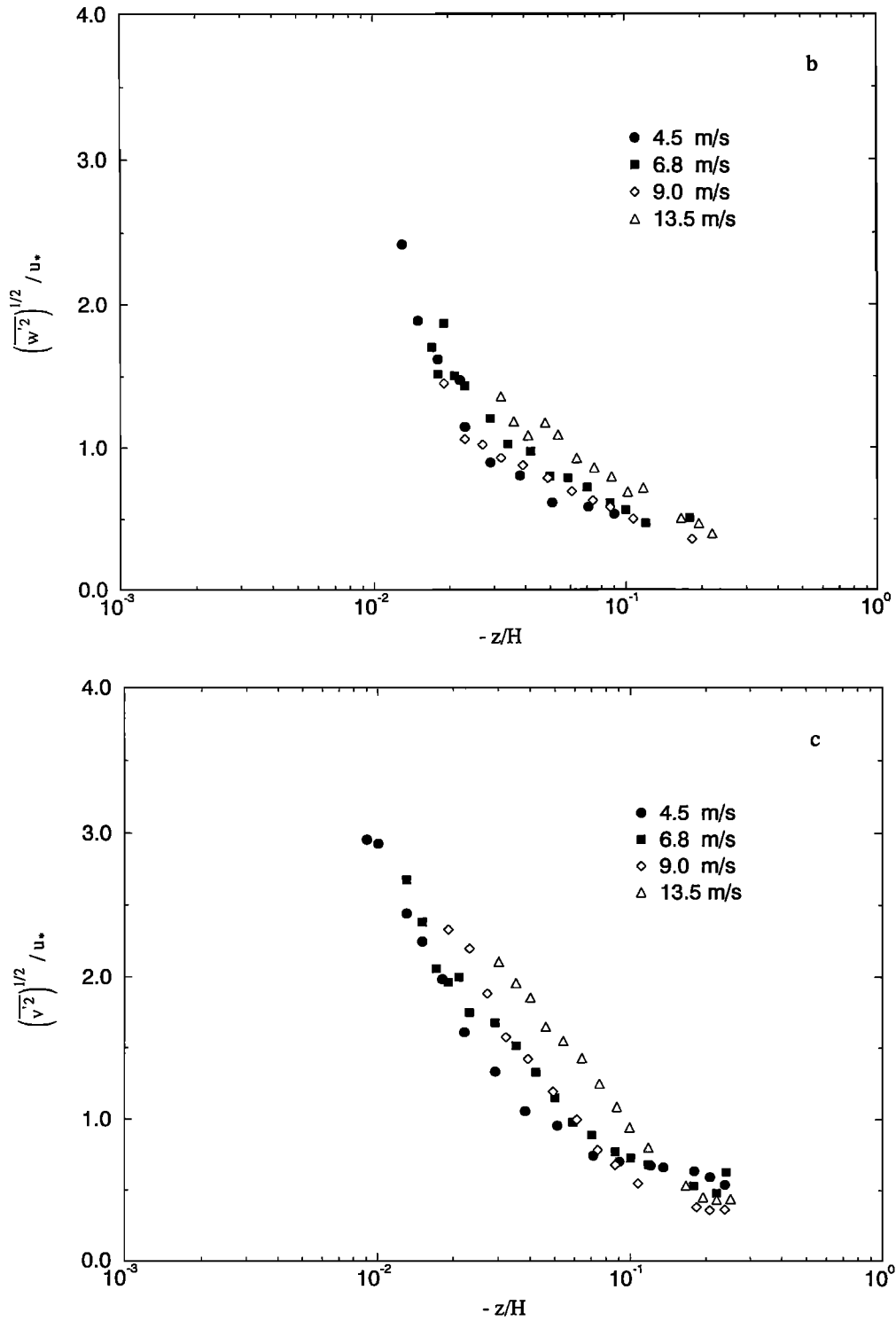


Figure 7. (continued)

very small nonlinear terms involving \tilde{v}_R (rejected in the turbulent motion in the second step of the TDM) or terms involving correlations of the type $\overline{\tilde{v}_i \tilde{v}'_j}$ which are nearly zero as explained in subsection 3.1. Neglecting these terms because of their smallness, the form of the balance equations obtained by phase averaging is conserved by the TDM; even the definition of \tilde{v} is different. Consequently, time-averaged kinetic energy balances for mean, orbital, and turbulent

motions write in the high Reynolds number limit [Reynolds and Hussain, 1972]

$$\frac{\overline{D}}{Dt} \left(\frac{1}{2} \overline{V_i V_i} \right) = \overline{\tilde{v}_i \tilde{v}_j} \frac{\partial \overline{V}_i}{\partial x_j} + \overline{\tilde{v}'_i \tilde{v}'_j} \frac{\partial \overline{V}_i}{\partial x_j} - \epsilon_M - \frac{\partial}{\partial x_j} \left[\frac{\overline{P}}{\rho} \overline{V}_j + \overline{V}_i (\overline{\tilde{v}_i \tilde{v}_j} + \overline{\tilde{v}'_i \tilde{v}'_j}) \right] \quad (2)$$

$$\frac{\overline{D}}{Dt} \left(\frac{1}{2} \overline{\tilde{v}_i \tilde{v}_i} \right) = -\overline{\tilde{v}_i \tilde{v}_j} \frac{\partial \overline{V}_i}{\partial x_j} + \overline{\tilde{v}_i \tilde{v}_j} \frac{\partial \overline{v}_i}{\partial x_j} - \varepsilon_w - \frac{\partial}{\partial x_j} \left[\frac{\overline{p'}}{\rho} \tilde{v}_j + \left(\overline{\tilde{v}_i \tilde{v}_j \tilde{v}_i} + \frac{1}{2} \overline{\tilde{v}_i \tilde{v}_i \tilde{v}_j} \right) \right] \quad (3)$$

$$\frac{\overline{D}}{Dt} \left(\frac{1}{2} \overline{v_i v_i} \right) = -\overline{v_i v_j} \frac{\partial \overline{V}_i}{\partial x_j} - \overline{v_i v_j} \frac{\partial \overline{v}_i}{\partial x_j} - \varepsilon_T - \frac{\partial}{\partial x_j} \left[\frac{\overline{p'}}{\rho} v_j + \left(\frac{1}{2} \overline{v_i v_i v_j} + \frac{1}{2} \overline{v_i v_j v_i} \right) \right] \quad (4)$$

In these equations, $\overline{D}/Dt = \partial/\partial t + \overline{V}_j \partial/\partial x_j$ and $\varepsilon_M, \varepsilon_w$, and ε_K denote the dissipation rates of $1/2 \overline{V_i V_i}$, $1/2 \overline{v_i v_i}$, and $1/2 \overline{v_i v_j}$, respectively. The $\overline{v_i v_j}$ represents the components of the wave-induced Reynolds stress tensor, i.e., the part of the Reynolds stress tensor $v_i v_j$ having a phase correlation with η .

The first term in the right-hand side of (2) and (3) represents energy transfers between the orbital motion and the mean flow. This term is the exact analog of the usual production term in the turbulent kinetic energy balance. Since the mean flow behaves mainly as a one-dimensional shear flow, this term is dominated by $\overline{u \tilde{w}} \partial U/\partial z$. As $\overline{u \tilde{w}}$ is zero for a purely potential orbital motion, it appears clearly that the orbital rotational motion plays a crucial role in wave-mean flow interactions. The second term in the right-hand side of (4), which appears with an opposite sign in (3), represents wave-induced turbulence production. This term was analyzed by *Kitaigorodskii and Lumley* [1983] in the case of irrotational waves, and these authors concluded it was negligible. However, if a rotational contribution with a strong vertical gradient exists in the orbital motion, this term may contribute significantly to the turbulent kinetic energy budget. Furthermore, since (2) involves both correlations $\overline{u \tilde{w}}$ and $\overline{u' w'}$, the latter stress can be modified by the existence of the former. Thus the turbulent kinetic energy balance can also be affected indirectly by the orbital rotational motion through the usual turbulence production term $-\overline{u' w' \partial U/\partial z}$.

4.2. Wave-Mean Flow Energy Transfers

According to the previous remarks, the cross correlation $\overline{u \tilde{w}}$ is the key term governing wave-mean flow energy transfers. As a one-component probe was used in the present experiments, we were unable to compute exactly the correlation $\overline{u \tilde{w}}$. However, since $\overline{u_R \tilde{w}_R}$ and $\overline{v_{P1} \tilde{v}_{Rj}}$ are presumably very small, one can write approximately

$$\overline{u \tilde{w}} = \overline{u_{P1} \tilde{w}_R} + \overline{u_R \tilde{w}_{P1}} \quad (5)$$

Both terms of the right-hand side of (5) can be computed using (29) of TM, and their vertical decay is shown in Figures 8a and 8b. The term $\overline{u_R \tilde{w}_{P1}}$ is seen to decrease monotonically when U_∞ increases, while $\overline{u_{P1} \tilde{w}_R}$ exhibits a more complex behavior. In contrast with $\overline{u_R \tilde{w}_{P1}}$, which is positive for all wind speeds, $\overline{u_{P1} \tilde{w}_R}$ is negative, except for the intermediate wind $U_\infty = 6.8$ m/s. It can be easily seen that the sum $\overline{u_{P1} \tilde{w}_R} + \overline{u_R \tilde{w}_{P1}}$ follows the sign of $\overline{u_{P1} \tilde{w}_R}$. This means that the energy transfer term in (3) is positive, except for $U_\infty = 6.8$ m/s, where energy goes from the orbital flow to the mean current. No satisfying explanation has been found for this singular case, even if negative production is not an uncommon feature

in turbulent flows, especially when nearly two-dimensional vortices are present.

Importance of the wave-mean flow transfer is perhaps better appreciated by comparison with the more familiar turbulence production, i.e., the first term in the right-hand side of (4). The ratio $R^2 = (\overline{u_{P1} \tilde{w}_R} / u_*^2)$ varies roughly from 85 at $U_\infty = 4.5$ m/s to 25 at $U_\infty = 13.5$ m/s. The ratio $-(\overline{u_{P1} \tilde{w}_R} + \overline{u_R \tilde{w}_{P1}}) / u_*^2$ evaluated near the surface thus varies from nearly 2.0 at $U_\infty = 4.5$ m/s to 0.5 at $U_\infty = 13.5$ m/s and takes the large negative value -3.0 at $U_\infty = 6.8$ m/s. These values show that energy transfers between mean current and orbital motion can be at least of the same order as the usual turbulence production. Their relative magnitude decreases at high wind velocities as does R^2 because, at least for young waves, the shear stress increases faster with wind speed than does the wave energy (see Table 1).

Present results can be compared with those obtained differently by previous authors. *Jiang et al.* [1990] did not separate the orbital rotational motion from turbulence. Thus the "turbulent" motion v_T defined by these authors corresponds to $\tilde{v}_R + v'$. However, since $\overline{v_{P1} v'_j} = 0$, the correlations $\overline{v_{P1} v_{Tj}}$ they computed are nearly identical to $\overline{v_{P1} \tilde{v}_{Rj}}$. *Jiang et al.* [1990] found $\overline{u_R \tilde{w}_{P1}} > 0$, like in the present study, but obtained $\overline{u_{P1} \tilde{w}_R} < 0$ and of similar magnitude, so that the sum of both terms approximately cancelled. Using a phase-averaging technique, *Cheung and Street* [1988] computed $\overline{u \tilde{w}}$ for periodic waves sheared by the wind and found this correlation positive at all wind speeds, indicating that energy is transferred from the orbital motion to the mean flow. In contrast, in their field measurements, *Cavaleri and Zecchetto* [1987] reported negative cross correlations whose magnitude was about 2 orders larger than surface stress. The only overall agreement emerging from this brief review is the existence of significant wave-mean flow energy transfers. However, depending on flow conditions, it appears that these transfers can change sign. Thus explaining the sign of $\overline{u \tilde{w}}$ is of great importance, and some indications about this point will be given in section 5.

4.3. An Indirect Identification of the Turbulence Source: The Dissipation Rate

The levels of $(\overline{u'^2})^{1/2}/u_*$ and $(\overline{w'^2})^{1/2}/u_*$ found in the present experiments suggest that turbulence production is mainly due to the mean shear. To get additional indications about a possible signature of wave-turbulence interactions in the turbulent motion, it is of particular interest to obtain an estimate of the dissipation rate ε_T . Such an estimate was performed in several field experiments. *Jones* [1985] carried out velocity measurements under strong wind conditions in the Bass Strait. Using the usual Taylor hypothesis, he estimated ε_T and found that the wall scaling $\varepsilon_T(z) \propto u_*^3/z$ applied. This contrasts with two different series of measurements performed on Lake Ontario by *Kitaigorodskii et al.* [1983] and *Agrawal et al.* [1992]; these authors found levels of ε_T larger by nearly 2 orders of magnitude than predicted by the law of the wall, a result suggesting that near-surface turbulence is dramatically enhanced by wave breaking.

A simple way for evaluating ε_T is to use the inertial subrange of the frequency spectra combined with a suitable Taylor hypothesis. As already mentioned, *Lumley and Terray* [1983] derived the relation between wave number spectra and frequency spectra when both mean current and orbital motion act to convect frozen isotropic turbulence past a fixed point.

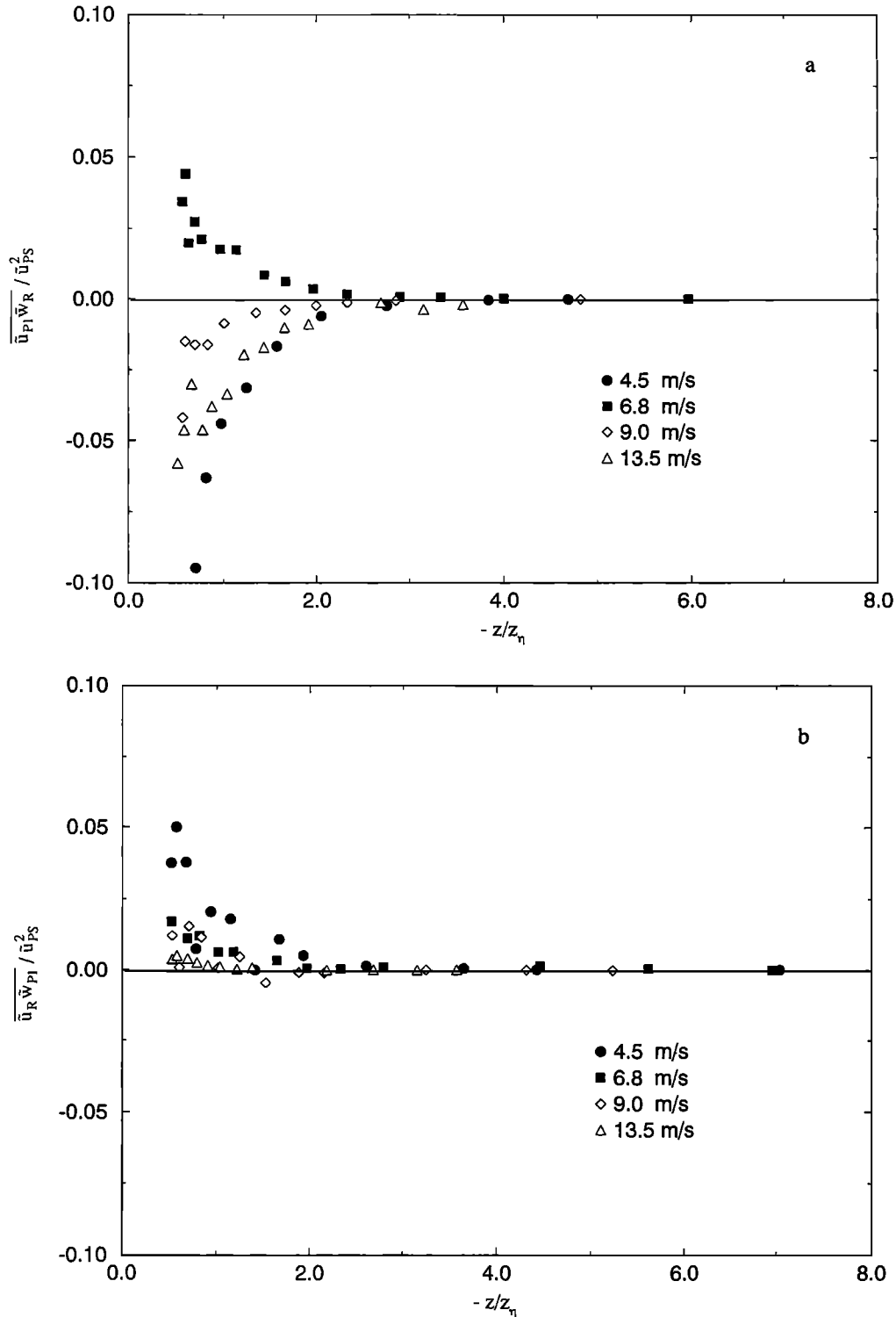


Figure 8. Vertical profiles of (a) $\overline{u_{p1} w_R} / \overline{u_{p1}^2}$ and (b) $\overline{u_R w_{p1}} / \overline{u_{p1}^2}$.

In the inertial subrange, according to their theory, frequency spectra of the streamwise fluctuation behave asymptotically at a given depth z as

$$S_{u' u'}(f, z) = \frac{9}{55} C_K (\overline{U}(z) \varepsilon_T)^{2/3} (2\pi f)^{-5/3} \quad f < f_0 \quad (6a)$$

$$S_{u' u'}(f, z) = \frac{7}{110} 2^{1/3} \Gamma\left(\frac{1}{3}\right) C_K (\overline{u_{p1}} \varepsilon_T)^{2/3} (2\pi f)^{-5/3} \quad f > f_0 \quad (6b)$$

where C_K is the Kolmogorov constant (hereinafter set to 1.5). As indicated, the well-known form (6a) is suitable for the part of the inertial range covering frequencies much smaller than the dominant wave frequency f_0 , while (6b), in which turbulence is convected by the orbital motion, applies far above f_0 . The measurements of *Kitaigorodskii et al.* [1983] indicate that both regions of the inertial subrange exist in spectra obtained from field data. The situation is somewhat different in laboratory experiments because the ratio between the dominant

wavelength and the scales of the energy-containing eddies is not the same due to short-fetch conditions. Examining our data, it appears that near the surface, the inertial subrange can be clearly identified only for $f > f_0$. In contrast, when depth increases, turbulent length scales grow rapidly and the inertial subrange shifts to lower frequencies, as shown by Figure 6. Owing to this trend, far from the surface, nearly all the inertial subrange lies at frequencies lower than f_0 . The determination of ε_T is achieved using expressions (6a) or (6b) according to the foregoing remarks. Only spectra presenting a substantial $f^{-5/3}$ zone have been used. Furthermore, u' spectra have been preferred to w' spectra because they present the strongest bump, allowing a more precise estimate of the bounds of the inertial subrange. The nondimensional dissipation rate $\kappa|z|\varepsilon_T/u_*^3$ determined this way is plotted on Figure 9 (the Von Karman constant κ is set equal to 0.4). The results show a fairly good agreement with the law of the wall, even if the intermediate case $U_* = 6.8$ m/s exhibits a different behavior as already observed for wave-mean flow energy transfers. The agreement is particularly good for the two highest wind speeds. Wave breaking is undoubtedly present in these cases but has no clearly discernible influence, even at the points closest to the surface, possibly because dissipation due to breaking is not injected in the inertial subrange used to compute ε_T . Overall, even though many possible sources of error exist in these estimates of ε_T , the results reinforce the conclusion that under present laboratory conditions, turbulence is not significantly affected by the orbital motion and remains controlled by the surface shear stress.

5. Possible Origins of the Orbital Rotational Motion

5.1. Theoretical Background

Having demonstrated experimentally the importance of the rotational part of the orbital motion in energy transfers, a fundamental question arises concerning the origin of \tilde{v}_R . Several dynamic processes can contribute to the generation of \tilde{v}_R , and they can be classified within two categories. One concerns the direct coupling between the air flow and the water motion through boundary conditions. The other regroups the distortions imposed to an orbital motion superimposed on a turbulent shear flow.

The first kind of mechanism can be summarized as follows. When the wave slope becomes significant, the boundary layer above the waves is distorted and a significant wave-induced contribution appears in the air motion. Owing to the high shear rate existing in the boundary layer, this contribution is strongly rotational. Thus matching conditions through the air-water interface imposes a nonzero, wave-induced spanwise vorticity $\tilde{\omega}_y$ at the water surface. Longuet-Higgins [1953, 1969] studied the modifications of the flow below a periodic wave in the presence of a nonzero surface value of $\tilde{\omega}_y$, resulting from the matching of the shear stresses. He emphasized the importance of the wave-induced surface vorticity in the creation of second-order drift currents which develop over the whole depth of the flow and showed that if the wave slope is small, then the vorticity balance imposes a very rapid vertical decay of $\tilde{\omega}_y$. More precisely, he determined that the boundary layer in which $\tilde{\omega}_y$ diffuses has a typical thickness $\delta = (2\nu/\omega)^{1/2}$ (ν being the kinematic viscosity of the water and ω the radian frequency of the wave). Phillips and Banner [1974] showed that in the top millimeters below the surface, nonlinear terms

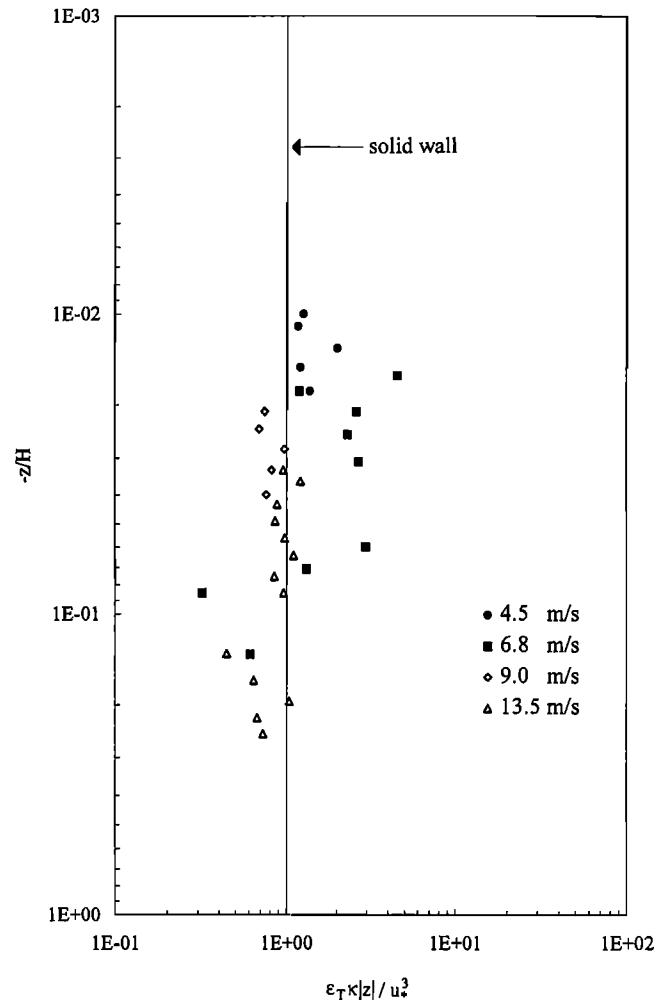


Figure 9. Nondimensional turbulent dissipation.

of the vorticity balance induce a dramatic increase of \tilde{u} below the crest when the wave slope goes beyond 0.2. Nevertheless, the laboratory wind waves we analyze here have typical slopes around 0.15, so that the linearization of the vorticity equation carried out by Longuet-Higgins [1953, 1969] seems applicable. Of course, his analysis did not take into account turbulence. However, in most laboratory experiments, water friction velocities are so that the characteristic viscous length ν/u_* exceeds δ . Thus it does not seem that turbulence can increase significantly the diffusion of $\tilde{\omega}_y$ from the surface. If the previous line of reasoning is correct, then one can conclude that the rotational component of the orbital motion generated at the surface through matching conditions with the air flow is necessarily confined to the immediate vicinity of the surface. Consequently, it does not seem realistic that this mechanism is responsible from the observations made in laboratory experiments far below this sublayer. The conclusion might be different in the field because the typical radian frequency ω is 1 order smaller than in laboratory experiments, making ν/u_* and δ comparable. Thus in that case, turbulence can perhaps attenuate significantly the vertical decay of $\tilde{\omega}_y$, which would then keep a significant value on a larger depth.

The key idea of the second group of mechanisms is that when a surface wave field is superimposed on a turbulent shear flow, the wave motion cannot remain strictly irrotational. This is simply a consequence of the nonlinearity of the equa-

tions of motion which leads to different sources of wave-induced vorticity. To define these sources, it is necessary to write the wave-induced vorticity balance. In the case of a periodic wave, denoting by $\overline{\omega}_i = \varepsilon_{ijk} \partial \overline{V}_k / \partial x_j$ the i th component of the mean vorticity and phase averaging yields,

$$\begin{aligned} \overline{\omega}_{i,t} + \overline{V}_j \frac{\partial \overline{\omega}_i}{\partial x_j} + \overline{v}_j \frac{\partial \overline{\omega}_i}{\partial x_j} &= \overline{\omega}_j \frac{\partial \overline{v}_i}{\partial x_j} + \overline{\omega}_j \frac{\partial \overline{V}_i}{\partial x_j} \\ + \overline{v}_j \frac{\partial \overline{\omega}_i}{\partial x_j} - \overline{v}_j \frac{\partial \overline{\omega}_i}{\partial x_j} - \overline{\omega}_j \frac{\partial \overline{v}_i}{\partial x_j} + \overline{\omega}_j \frac{\partial \overline{v}_i}{\partial x_j} &- \varepsilon_{ijk} \frac{\partial^2}{\partial x_j \partial x_k} \overline{v}_i \overline{v}_j \end{aligned} \quad (7)$$

This equation shows that if $\overline{\omega}_i$ is initially zero as in the case for irrotational waves, it remains zero only if the three possible source terms (the terms that do not contain $\overline{\omega}_i$) are zero. The first one, $\overline{v}_j \partial \overline{\omega}_i / \partial x_j$, is different from zero if the mean shear is nonuniform, as observed below wind waves where $\partial^2 \overline{U} / \partial z^2$ is nonzero. The second one, $\overline{\omega}_j \partial \overline{v}_i / \partial x_j$, exists when the wave field is three-dimensional or when the mean current is nonuniform in the spanwise direction. It is this term that is responsible for the generation of Langmuir cells through the two mechanisms analyzed by *Craik and Leibovich* [1976] and *Craik* [1977]. The last possible source term is related to the wave-induced Reynolds stress tensor $\overline{v}_i \overline{v}_j$ and will be discussed below.

Under suitable assumptions, (7) can be linearized and solved by means of asymptotic expansions. Then, the normal mode solution $\overline{\omega}_i$ can be integrated to obtain explicit expressions of the rotational components of the orbital motion \overline{u}_R and \overline{w}_R [Magnaudet and Masbernat, 1990]. For example, assuming a two-dimensional flow and disregarding all terms in the right-hand side of (7) leads to the creation of a streamwise component $\overline{u}_R^{(1)}$ given near the surface by

$$\overline{u}_R^{(1)} \approx - \frac{\overline{u}_P}{k[c - \overline{U}(z)]} \frac{\partial \overline{U}}{\partial z} \quad (8)$$

From (8) it can be deduced that

$$\overline{\overline{u}_R^{(1)} \overline{u}_P} \approx - \frac{\overline{u}_P^2}{k[c - \overline{U}(z)]} \frac{\partial \overline{U}}{\partial z} \quad (9)$$

$$\overline{\overline{w}_P \overline{w}_R^{(1)}} \approx - \frac{\overline{w}_P^2}{[c - \overline{U}(z)]} (\overline{U}(z) - U_0) \quad (10)$$

$$\overline{\overline{u}_R^{(1)} \overline{w}_P} = 0 \quad (11a)$$

$$\overline{\overline{u}_P \overline{w}_R^{(1)}} = 0 \quad (11b)$$

Equations (9) and (10) show that the term $\overline{v}_j \partial \overline{\omega}_i / \partial x_j$, which is entirely responsible for the creation of the spanwise vorticity $\overline{\omega}_i$ in this simplified model, creates substantial correlations between the potential and rotational contributions. However, as shown by (11a)-(11b), this mechanism cannot explain the origin of wave-mean flow energy transfers.

The vortex-stretching term $\overline{\omega}_j \partial \overline{v}_i / \partial x_j$ is a possible candidate for the generation of a wave-induced shear stress

when the wave field is strongly three-dimensional; *Gartshore et al.* [1983] studied the evolution of an initially irrotational three-dimensional random motion interacting with a mean shear $\partial \overline{U} / \partial z$. They showed that owing to this vortex-stretching mechanism, a shear stress develops in time. However, since the waves we are studying experimentally are nearly two-dimensional, this mechanism is probably of little importance in the present context, except perhaps at the highest wind speed.

Unlike the other source terms, $\overline{v}_i \overline{v}_j$ has to be modeled before its effects can be discussed. The closure of $\overline{v}_i \overline{v}_j$ is a very difficult problem, which is still open, in spite of numerous attempts (see *Davis* [1974] and *Townsend* [1980]). The difficulty comes from the fact that one part of $\overline{v}_i \overline{v}_j$ is in phase with the wave-induced strain rate $\overline{S}_{ij} = 1/2(\partial \overline{v}_i / \partial x_j + \partial \overline{v}_j / \partial x_i)$ and is of dissipative nature, whereas the other part is 90° out of phase with \overline{S}_{ij} and represents the elastic response of turbulence to the periodic distortion imposed by the orbital motion. For example, a closure based on a generalized eddy viscosity $\nu_T = \overline{\nu}_T + \overline{\tilde{\nu}_T}$ can be formulated as [Fua et al., 1982]

$$\overline{v}_i \overline{v}_j - \frac{1}{3} \overline{v}_i^2 \delta_{ij} = -2 \left(\overline{\nu}_T \overline{S}_{ij} + \overline{\tilde{\nu}_T} \overline{S}_{ij} + \overline{\tilde{\nu}_T} \overline{S}_{ij} - \overline{\tilde{\nu}_T} \overline{S}_{ij} \right) \quad (12)$$

where \overline{S}_{ij} denotes the mean strain rate. When included into (7), expression (12) shows that $\overline{v}_i \overline{v}_j$ can contribute to the creation of $\overline{\omega}_i$ through several terms. All possible terms exist below wind waves; some of them result from the inhomogeneity of the turbulence (represented schematically by the vertical gradient of ν_T), while others are due to the inhomogeneity of the mean shear \overline{S}_{ij} . The important feature about the contribution $\overline{\overline{u}_R^{(2)}}, \overline{\overline{w}_R^{(2)}}$ induced by $\overline{v}_i \overline{v}_j$ is that it creates cross correlations $\overline{\overline{u}_R^{(2)} \overline{w}_P}$ and $\overline{\overline{u}_P \overline{w}_R^{(2)}}$. For example, the first term in the right-hand side of (12) creates a source term in the $\overline{\omega}$ balance. This term which relates to the "viscous" response of water turbulence to the distortion provided by the orbital motion $\overline{\nu}_T$ leads to [Magnaudet, 1989; Magnaudet and Masbernat, 1990]

$$\overline{\overline{u}_R^{(2)} \overline{w}_P} \approx -2 \overline{\nu}_{T,x} \frac{\overline{w}_P^2}{[c - \overline{U}(z)]} \quad (13)$$

As discussed in section 4, such cross correlations affect directly the energy balances of both mean and orbital motions. They can also affect in an indirect manner the turbulent kinetic energy balance; *Magnaudet and Masbernat* [1990] showed that the wave-induced stress given by (13) combined with the mean momentum balance could explain quantitatively the very high level of turbulence measured below periodic waves by *Cheung and Street* [1988]. However, it must be stressed that any conclusion about the role of $\overline{v}_i \overline{v}_j$ in (7) is entirely dependent on the validity of the closure assumption formulated for this tensor. For example, on the basis of timescale arguments, *Belcher et al.* [1994] have shown that the eddy viscosity assumption leading to (13) is only valid in a very thin layer of water beneath the surface. In the deeper region, turbulence is not in a local equilibrium state; it exhibits essentially an elastic behavior that has to be modeled through rapid distortion theory. All this suggests that much theoretical work is needed for closing accurately $\overline{v}_i \overline{v}_j$ before drawing definite conclusions about the role of wave-induced Reynolds stresses in wave-current and wave-turbulence interactions.

To summarize this section, it appears that in laboratory studies the wave characteristics are such that the curvature of the mean current $\partial^2 \bar{U} / \partial z^2$ and the wave-induced Reynolds stresses $\bar{v}_i \bar{v}_j$ are probably the main sources of orbital rotational motion. However, the conclusion is certainly markedly different in field situations since the mean current plays a less decisive role, while three-dimensional effects and perhaps direct coupling with the air flow are more significant.

5.2. Experimental Indications

In order to check the mechanisms previously discussed, it seems very appropriate to compare the correlations $\bar{v}_{Pi} \bar{v}_{Rj}$ determined from measurements to those predicted theoretically. The major limitation of this approach is, of course, that it is restricted to the expressions involving solely measurable quantities. As a consequence, expressions like (13) involving modeling of the wave-induced Reynolds stress tensor cannot be checked and no additional information about the generation of the crucial cross correlation $\bar{u} \bar{w}$ can be obtained this way. Thus only correlations $\bar{u}_{Pi} \bar{u}_R$ and $\bar{w}_{Pi} \bar{w}_R$ are discussed in the following. Figures 10a and 10b depict the behavior of these two correlations. The most remarkable feature is that $\bar{u}_{Pi} \bar{u}_R$ is very generally negative, while $\bar{w}_{Pi} \bar{w}_R$ is positive, except for the lowest wind speed. Turning back to (9)-(10), it appears that this theoretical model predicts $\bar{u}_{Pi} \bar{u}_R < 0$ and $\bar{w}_{Pi} \bar{w}_R > 0$ since $\partial \bar{U} / \partial z > 0$ and $\bar{U}(z) - U_0 < 0$. The specific behavior of $\bar{w}_{Pi} \bar{w}_R$ at the lowest wind speed cannot be explained this way, but the agreement in all other cases suggests to check whether the intensity of the correlations predicted by (9)-(10) is realistic or not. Since these theoretical predictions have been obtained by neglecting completely turbulent diffusion in (7), they can at best give an estimate in the region where $\tilde{\omega}$ is produced. That is the reason why predicted and computed correlations are compared only at the measured point closest to the surface. The comparison is achieved by assuming that the dominant wave contains all the wave energy and by fitting the mean current profiles with logarithmic curves. Results of this comparison are summarized in Table 2. Theoretical expressions generally overestimate the correlations obtained from experiments by a factor varying between 1 and 2. However, they respect the order of magnitude and the tendencies displayed by experimental results. Considering all sources of error in both theoretical and "experimental" evaluations, the result is quite encouraging and shows the prominent role played by wave-current interactions in the generation of \tilde{v}_R in laboratory experiments. Very different experiments carried out by *Rashidi et al.* [1992] also provide an interesting indication. These authors visualized and analyzed the vorticity field in a free-surface channel flow forced by long waves and found that strong negative vorticities occurred below wave crests, whereas positive vorticities were found below the troughs. This is exactly what is predicted by (8), even though the origin of the mean shear differs in free-surface channel flows and in wind-driven flows.

5.3. About the nature of \tilde{v}_R

As shown before, in our experiments one of the most important mechanisms in the generation of \tilde{v}_R appears to be basically a wave-current interaction: wave-induced potential motion combined with inhomogeneous mean shear leads to the term $\tilde{v}_j \partial \bar{\omega}_i / \partial x_j$ in (7), and for this term to be balanced a wave-induced vorticity is created. This mechanism has

nothing to do with turbulence. However, for wind waves, \tilde{v}_P is random and this randomness is reflected in the distribution of \tilde{v}_R as shown by the spectra of Figure 4. Thus in this flow a random and nearly two-dimensional motion correlated with wave elevation and carrying vorticity is superimposed on turbulent fluctuations. The question that comes to mind is then whether \tilde{v}_R can be classified as turbulent or not.

As pointed out before, *Jiang et al.* [1990] did not identify \tilde{v}_R . They separated the orbital motion \tilde{v} defined as the potential contribution \tilde{v}_P from the remaining fluctuation $\tilde{v}_R + v'$ defined as turbulence. As a consequence of their definition of the turbulent motion, *Jiang et al.* [1990] wrote a balance equation of the turbulent kinetic energy different from (4) by several terms involving the correlation tensor $(v'_i + \tilde{v}_{Ri}) \tilde{v}_{Pj}$. For example, a production term $-(\bar{u}' + \bar{u}_R) \bar{w}_P \partial \bar{U} / \partial z$ appeared, and the authors found it to be of very significant intensity, not an unlikely result if we refer to the significant correlation $\bar{u}_R \bar{w}_P$ found in the present experiments. *Jiang et al.* [1990] concluded that these features proved that significant wave-turbulence interactions were present in their results. Surprisingly, the profiles they found for the "turbulent" intensities agreed well with the well-known boundary layer results [*Klebanoff*, 1955] as if there were no wave-turbulence interactions. This paradox is solved if \tilde{v}_R is not included into the turbulent motion but is rather seen as a part of the orbital contribution; the turbulent kinetic energy balance then reduces to (4), and *Jiang et al.* found that in their experiments the extra production term of (4) was negligible. In such a case, (4) reduces to the usual balance and no fundamental contradiction appears with the results obtained for the turbulent moments.

Inclusion of \tilde{v}_R as a part of the orbital motion rather than a turbulent contribution is, in fact, basically suggested by the essentially two-dimensional nature of \tilde{v}_R , which makes this motion very different from three-dimensional, dissipative turbulent motions. The picture of the wave-induced motion that emerges from both theoretical analysis and laboratory experiments is that of a coherent motion induced mainly by interactions between a forced excitation (the surface waves) and the mean flow; owing to these interactions, the orbital motion carries its own vorticity $\tilde{\omega}$ and remains coherent over long times or distances because of its correlation to wave elevation. These properties are basically those frequently used to define coherent structures [*Hussain*, 1983]. However, in the present case it must be kept in mind that unlike the usual situation regarding coherent structures, no instability mechanism is needed for the generation of $\tilde{\omega}$. Analogy with coherent structures was also suggested for mechanical waves by *Cheung and Street* [1988], who obtained $\bar{u} \bar{w} > 0$ with such waves; positive cross correlations leading to the so-called negative production phenomenon occur frequently when coherent structures are present [*Hussain*, 1981].

The question of the classification of \tilde{v}_R is more than a semantic problem and can have implications in modeling of turbulent flows below wind waves; turbulence models are generally unable to describe motions involving length and timescales of different natures, and accurate modeling is probably only possible if the whole orbital velocity field and the turbulent motion which are governed by completely different dynamics are described separately.

6. Conclusions

Our aim in this work was to present some new experimental insights about wave-current and wave-turbulence interactions

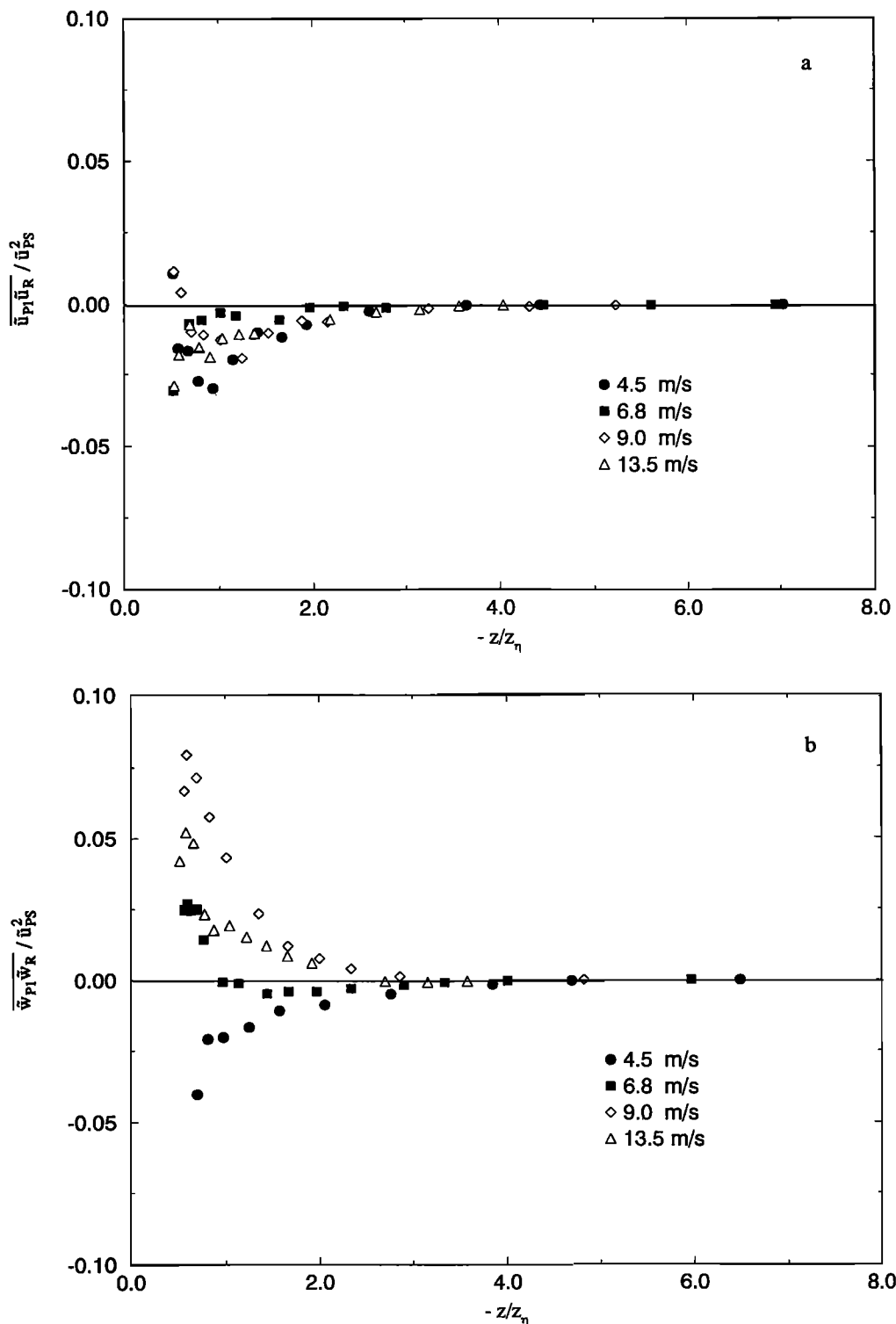


Figure 10. Vertical profiles of (a) $\overline{u_{p1}u_R}$ and (b) $\overline{w_{p1}w_R}$.

below laboratory wind waves. New experimental data were obtained, and they were processed using the triple decomposition method which allows one to isolate both potential and rotational contributions of the orbital motion from turbulent fluctuations. Analysis of present results reveal the following:

1. The orbital rotational motion is of significant magnitude; in our experiments it reaches between 20 and 30% of the orbital potential contribution.

2. Cross-correlations $\overline{u_{p1}w_R}$ and $\overline{u_Rw_{p1}}$ can induce important energy transfers between the mean flow and the wave-induced flow. The sign of these transfers can change with wind speed, and their magnitude is related to the ratio R^2 between the kinetic energy of the orbital motion and the surface shear.

3. In these experiments, turbulent intensities are of the same order of magnitude as those found in usual boundary layers, but they exhibit a different vertical decay probably related to the existence of streamwise vortices in our facility.

Table 2. Correlations $\overline{\tilde{u}_{P1}\tilde{u}_R}$ and $\overline{\tilde{w}_{P1}\tilde{w}_R}$: Comparison Between Theory and Experiment

U_∞ , m/s	4.5	6.8	9.0	13.5
$(\overline{\tilde{u}_{P1}\tilde{u}_R} / \overline{\tilde{u}_{P1}^2})_{\text{exp}}$	-0.053	-0.105	-0.074	-0.098
From equation (8)	-0.060	-0.178	-0.102	-0.198
$(\overline{\tilde{w}_{P1}\tilde{w}_R} / \overline{\tilde{w}_{P1}^2})_{\text{exp}}$	-0.125	0.088	0.200	0.194
From equation (9)	0.064	0.145	0.235	0.267

Estimates of the dissipation rate confirm that turbulent quantities scale as in usual wall-bounded flows.

4. Most of the properties displayed by correlations $\overline{\tilde{u}_{P1}\tilde{u}_R}$ and $\overline{\tilde{w}_{P1}\tilde{w}_R}$ are predicted by a theoretical model in which \tilde{v}_R is produced by a wave-current interaction due to the vertical variations of the mean shear. However, this conclusion is probably specific to laboratory waves, and several other mechanisms which are certainly more important in the ocean have been suggested.

Present results show that the orbital rotational motion is a cornerstone for understanding wave-current interactions. Theoretical arguments suggest that it probably plays also a key role in wave-turbulence interactions. It is thus highly desirable that conceptual models and separation methods be improved in order to get more information about vorticity dynamics below wind waves. Furthermore, no significant effect of the waves on the turbulent motion was found in the present study, probably because the kinetic energy of the orbital motion was not sufficient. It is thus crucial that new laboratory experiments involving more energetic waves be performed to clarify the mechanisms of wave-turbulence interactions.

Acknowledgments. This research was partly supported by the French PAMOS Program under grants n° 91 / ATP / 631 and 92N50 / 0268.

References

- Agrawal, Y.C., E.A. Terray, M.A. Donelan, P.A. Hwang, A.J. Williams, W.M. Drennan, K.K. Kahma, and S.A. Kitaigorodskii, Enhanced dissipation of kinetic energy beneath surface waves, *Nature*, 359, 219-220, 1992.
- Belcher, S.E., J.A. Harris, and R.L. Street, Linear dynamics of wind waves in coupled turbulent air-water flow, 1, Theory, *J. Fluid Mech.*, 271, 119-151, 1994.
- Benilov, A. Yu., and B.N. Filyushkin, Application of methods of linear filtration to an analysis of fluctuations in the surface layer of the sea, *Izv. Acad. Sci. USSR Atmos. Oceanic Phys., Engl. transl.*, 6, 477-482, 1970.
- Cavaleri, O., and S. Zecchetto, Reynolds stresses under wind waves, *J. Geophys. Res.*, 92(C4), 3894-3904, 1987.
- Cheung, T.K., and R.L. Street, Turbulent layers in the water at an air-water interface, *J. Fluid Mech.*, 194, 133-151, 1988.
- Craik, A.D.D., The generation of Langmuir circulations by an instability mechanism, *J. Fluid Mech.*, 81, 209-223, 1977.
- Craik, A.D.D., and S. Leibovich, A rational model for Langmuir circulations, *J. Fluid Mech.*, 73, 401-426, 1976.
- Davis, R.E., Perturbed turbulent flow, eddy viscosity and the generation of turbulent stresses, *J. Fluid Mech.*, 63, 673-693, 1974.
- Dean, R.G., Stream function representation of nonlinear ocean waves, *J. Geophys. Res.*, 70(18), 4561-4572, 1965.
- Donelan M.A., Whitecaps and momentum transfer, in *Turbulent Fluxes Through the Sea Surface, Wave Dynamics, and Prediction*, edited by A. Favre and K. Hasselmann, pp. 273-287, Plenum, New York, 1978.
- Fua, D., G. Chimonas, F. Einaudi, and O. Zeman, An analysis of wave-turbulence interaction, *J. Atmos. Sci.*, 39, 2450-2463, 1982.
- Gartshore, I.S., P.A. Durbin, and J.C.R. Hunt, The production of turbulent stress in a shear flow by irrotational fluctuations, *J. Fluid Mech.*, 137, 307-329, 1983.
- Hussain, A.K.M.F., Role of coherent structures in turbulent shear flows, *Proc. Indian Acad. Sci.*, 4 (2), 129-175, 1981.
- Hussain, A.K.M.F., Coherent structures: reality and myth, *Phys. Fluids*, 26(10), 2816-2850, 1983.
- Jiang, J.Y., R.L. Street, and S.P. Klotz, A study of wave-turbulence interaction by use of a nonlinear water wave decomposition technique, *J. Geophys. Res.*, 95(C9), 16,037-16,054, 1990.
- Jones, I.S.F., Turbulence below wind waves, in *The Ocean Surface*, edited by Y. Toba and H. Mitsuyasu, pp. 437-442, D. Reidel, Norwell, Mass., 1985.
- Kitaigorodskii, S.A.K., and J.L. Lumley, Wave-turbulence interactions in the upper ocean, I, The energy balance of the interacting fields of surface wind waves and wind-induced three-dimensional turbulence, *J. Phys. Oceanogr.*, 13, 1977-1987, 1983.
- Kitaigorodskii, S.A.K., M.A. Donelan, J.L. Lumley, and E.A. Terray, Wave-turbulence interactions in the upper ocean, II, Statistical characteristics of wave and turbulent components of the random velocity field in the marine surface layer, *J. Phys. Oceanogr.*, 13, 1988-1999, 1983.
- Klebanoff, P.S., Characteristics of turbulence in a boundary layer flow with zero pressure gradient, *Rep. 1247, Nat. Advis. Clee. Aero.*, Wash., 1955.
- Longuet-Higgins, M.S., Mass transport in water waves, *Philos. Trans. R. Soc. London A*, 535-581, 1953.
- Longuet-Higgins, M.S., Action of a variable stress at the surface of water waves, *Phys. Fluids*, 12(4), 737-740, 1969.
- Lumley, J.L., and E.A. Terray, Kinematics of turbulence convected by a random wave field, *J. Phys. Oceanogr.*, 13, 2000-2007, 1983.
- Magnaudet, J., Interactions interfaciales en écoulement à phases séparées, Thèse de Doctorat, Inst. Polytech. de Toulouse, Toulouse, France, 1989.
- Magnaudet, J., and L. Masbernat, Interactions des vagues de vent avec le courant moyen et la turbulence, *C.R. Acad. Sci. Paris, Sér. 2*, 1461-1466, 1990.
- Phillips, O.M., and M.L. Banner, Wave breaking in the presence of wind drift and swell, *J. Fluid Mech.*, 66, 625-640, 1974.
- Prodhomme, M.T., Turbulence sous les vagues de vent, Thèse de Doctorat, Inst. Polytech. de Toulouse, Toulouse, France, 1988.
- Rashidi, M., G. Hetsroni, and S. Banerjee, Wave-induced interaction in free-surface channel flows, *Phys. Fluids A*, 4 (12), 2727-2738, 1992.
- Reynolds, W.C., and A.K.M.F. Hussain, The mechanics of an organized wave in turbulent shear flow, 3, Theoretical model and comparisons with experiments, *J. Fluid Mech.*, 54 (2), 263-288, 1972.
- Terray, E.A., and L.F. Bliven, The vertical structure of turbulence beneath gently breaking wind waves, in *The Ocean Surface*, edited by Y. Toba and H. Mitsuyasu, pp. 395-400, D. Reidel, Norwell, Mass., 1985.
- Thais, L., and J. Magnaudet, A triple decomposition of the fluctuating motion below laboratory wind water waves, *J. Geophys. Res.*, this issue.
- Townsend, A.A., The response of sheared turbulence to additional distortion, *J. Fluid Mech.*, 81(1), 171-191, 1980.

J. Magnaudet and L. Thais, Institut de Mécanique des Fluides de Toulouse, 2 Avenue Camille Soula, 31400 Toulouse, France. (e-mail: magnau@imft.enseciht.fr; thais@imft.enseciht.fr)

(Received April 7, 1994; revised October 13, 1994; accepted October 13, 1994.)